Quantum-geometric perspective on spin-orbit-coupled Bose superfluids

A. L. Subaşı[1] and M. Iskin[2]

[1]*Department of Physics, Faculty of Science and Letters, Istanbul Technical University, 34469 Maslak, Istanbul, Turkey*

[2]*Department of Physics, Koç University, Rumelifeneri Yolu, 34450 Sarıyer, Istanbul, Turkey*

(Received 4 October 2021; accepted 19 January 2022; published 1 February 2022)

We employ the Bogoliubov approximation to study how the quantum geometry of the helicity states affects the superfluid properties of a spin-orbit-coupled Bose gas in continuum. In particular we derive the low-energy Bogoliubov spectrum for a plane-wave condensate in the lower helicity band and show that the geometric contributions to the sound velocity are distinguished by their linear dependences on the interaction strength; that is, they are in sharp contrast to the conventional contribution which has a square-root dependence. We also discuss the roton instability of the plane-wave condensate against the stripe phase and determine their phase-transition boundary. In addition we derive the superfluid density tensor by imposing a phase twist on the condensate order parameter and study the relative importance of its contribution from the interband processes that is related to the quantum geometry.

DOI: 10.1103/PhysRevA.105.023301

I. INTRODUCTION

Recent studies have shown that the quantum geometry of the Bloch states can play important roles in characterizing some of the fundamental properties of Fermi superfluids (SFs) [1,2]. The physical mechanism is quite clear in a multiband lattice: the geometric effects originate from the dressing of the effective mass of the SF carriers by the interband processes, which in return controls those SF properties that depend on the carrier mass. Besides the SF density and weight, the list includes the velocity of the low-energy Goldstone modes and the critical Berezinskii-Kosterlitz-Thouless temperature [1–8]. On the other hand, the intraband processes give rise to the conventional effects. It has been established that depending on the band structure and the strength of the interparticle interactions, the geometric effects can become sizable and may even dominate in an isolated flat band [1]. Furthermore, such geometric effects on Fermi SFs can be traced all the way back to the two-body problem in a multiband lattice in vacuum [9,10].

Despite the growing number of recent works exposing the role of quantum geometry in Fermi SFs, there is a lack of understanding of the bosonic counterparts which are much less studied [11–13]. For instance, Julku *et al.* considered a weakly interacting Bose-Einstein condensate (BEC) in a flat band and showed that the speed of sound has a linear dependence on the interaction strength and a square-root dependence on the quantum metric of the condensed Bloch state [11,12]. They also showed that the quantum depletion is dictated solely by the quantum geometry and the SF weight has a quantum-geometric origin.

Motivated by the success of analogous works on spin-orbit-coupled Fermi SFs [3–5,7], here we investigate the SF properties of a spin-orbit-coupled Bose gas from a quantum-geometric perspective. Our work differs from the existing literature in several ways [15–17]. In particular we derive the low-energy Bogoliubov spectrum for a plane-wave condensate in the lower helicity band and identify the geometric contributions to the sound velocity. The geometric effects survive only when the single-particle Hamiltonian has a σ_z term in the pseudospin basis that is coupled with a σ_x (and/or, equivalently, a σ_y) term. In contrast to the conventional contribution that has square-root dependence on the interaction strength, we find that the geometric ones are distinguished by linear dependence. Similar to the fermion problem in which the geometric effects dress the effective mass of the Goldstone modes, here one can also interpret the geometric terms in terms of a dressed effective mass for the Bogoliubov modes. We also discuss the roton instability of the plane-wave ground state against the stripe phase and determine the phase-transition boundary. All of these results are achieved analytically by reducing the 4×4 Bogoliubov Hamiltonian (which involves both lower and upper helicity bands) down to 2×2 by projecting the system onto the lower helicity band. The projected Hamiltonian works extremely well except for a tiny region in momentum space around the point where the helicity bands are degenerate. In addition we derive the SF density tensor by imposing a phase twist on the condensate order parameter and analyze the relative importance of its contribution from the interband processes [13].

The rest of this paper is organized as follows. We begin with the theoretical model in Sec. II: the many-body Hamiltonian is introduced in Sec. II A, and the noninteracting helicity spectrum is reviewed in Sec. II B. Then we present the Bogoliubov mean-field theory for a plane-wave condensate in Sec. III: the four branches of the full Bogoliubov spectrum are discussed in Sec. III A, and the two branches of the projected (i.e., to the lower helicity band) Bogoliubov spectrum are derived in Sec. III B. Furthermore, by analyzing the resultant Bogoliubov spectrum in the low-energy regime, we find closed-form analytic expressions for the Bogoliubov modes in Sec. III C and for the roton instability of the plane-wave condensate against the stripe phase in Sec. III D. Finally, we derive and analyze the SF density tensor and condensate density in Sec. IV. The paper ends with a summary of our conclusions in Sec. V.

II. THEORETICAL MODEL

In order to study the interplay between a BEC and spin-orbit coupling (SOC) and having cold-atom systems in mind, here we consider a two-component atomic Bose gas that is characterized by a weakly repulsive zero-range (contact) interaction in continuum. It is customary to refer to such a two-component bosonic system as the pseudospin-$\frac{1}{2}$ Bose gas.

A. Pseudospin-$\frac{1}{2}$ Bose gas

In particular, by making use of the momentum-space representation, we express the single-particle Hamiltonian in the usual form,

$$\mathcal{H}_0 = \sum_{\mathbf{k}} \Lambda_{\mathbf{k}}^\dagger \left[(\varepsilon_{\mathbf{k}} + \varepsilon_{\mathbf{k}_0})\sigma_0 + \frac{\mathbf{d}_{\mathbf{k}} \cdot \boldsymbol{\sigma}}{m} \right] \Lambda_{\mathbf{k}}, \tag{1}$$

where $\mathbf{k} = (k_x, k_y, k_z)$ is the momentum vector with $\hbar = 1$ and $\Lambda_{\mathbf{k}}^\dagger = (a_{\uparrow\mathbf{k}}^\dagger \; a_{\downarrow\mathbf{k}}^\dagger)$ is a two-component spinor with the creation operator $a_{\sigma\mathbf{k}}^\dagger$ for a pseudospin-σ particle in state $|\sigma\mathbf{k}\rangle = a_{\sigma\mathbf{k}}^\dagger|0\rangle$. Here $\sigma = \{\uparrow, \downarrow\}$ labels the two components of the Bose gas, and $|0\rangle$ is the vacuum state. The first term $\varepsilon_{\mathbf{k}} = k^2/(2m)$ is the kinetic energy of a particle, where $\varepsilon_{\mathbf{k}_0}$ is a convenient choice of an energy offset ($\mathbf{k_0}$ is defined below) and σ_0 is an identity matrix. The second term is the so-called SOC, where $\boldsymbol{\sigma} = (\sigma_x, \sigma_y, \sigma_z)$ is a vector of Pauli spin matrices and $\mathbf{d}_{\mathbf{k}} = (d_{\mathbf{k}}^x, d_{\mathbf{k}}^y, d_{\mathbf{k}}^z)$ is the SOC field with linearly dispersing components $d_{\mathbf{k}}^i = \alpha_i k_i$. Here we choose $\alpha_i \geqslant 0$ and $\alpha_x \geqslant \{\alpha_y, \alpha_z\}$ without the loss of generality.

Similarly, a compact way to express the intraspin and interspin interaction terms is

$$\mathcal{H}_U = \frac{1}{2V} \sum_{\substack{\sigma\sigma' \\ \mathbf{k_1}+\mathbf{k_2}=\mathbf{k_3}+\mathbf{k_4}}} U_{\sigma\sigma'} a_{\sigma\mathbf{k_1}}^\dagger a_{\sigma'\mathbf{k_2}}^\dagger a_{\sigma'\mathbf{k_3}} a_{\sigma\mathbf{k_4}}, \tag{2}$$

where V is the volume and $U_{\sigma\sigma'} \geqslant 0$ is the strength of the interactions. Here we consider a sufficiently weak $U_{\uparrow\downarrow}$ in order to prevent competing phases that are beyond the scope of this paper. See Sec. III D for a detailed account of the stability analysis. In addition we include a chemical potential term $\mathcal{H}_\mu = -\sum_{\sigma\mathbf{k}} \mu_\sigma a_{\sigma\mathbf{k}}^\dagger a_{\sigma\mathbf{k}}$ in the total Hamiltonian $\mathcal{H} = \mathcal{H}_0 + \mathcal{H}_U + \mathcal{H}_\mu$ of the system and determine μ_σ in a self-consistent fashion.

B. Helicity bands

Let us first discuss the single-particle ground state. The eigenvalues of the Hamiltonian matrix shown in Eq. (1) can be written as

$$\xi_{s\mathbf{k}} = \varepsilon_{\mathbf{k}} + \varepsilon_{\mathbf{k}_0} + s\frac{d_{\mathbf{k}}}{m}, \tag{3}$$

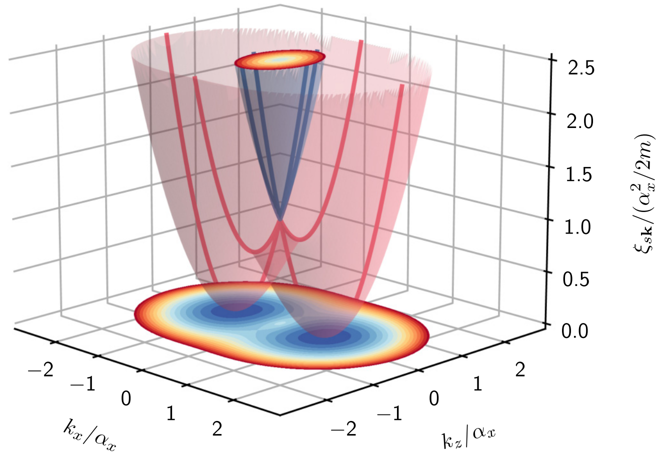

FIG. 1. Helicity bands $\xi_{s\mathbf{k}}$ (in units of $\alpha_x^2/2m$) are shown for $\alpha_x = 2\alpha_z$ and $\alpha_y = 0$ at $k_y = 0$. The upper red and lower blue bands touch at $\mathbf{k} = \mathbf{0}$. The single-particle ground state is doubly degenerate at $\mathbf{k} = (\pm\alpha_x, 0, 0)$.

where $s = \pm$ label, respectively, the upper and lower bands and $d_{\mathbf{k}} = |\mathbf{d}_{\mathbf{k}}|$ is the magnitude of the SOC field. Therefore, the single-particle (helicity) spectrum exhibits two branches due to SOC. In the pseudospin basis $|\sigma\mathbf{k}\rangle$, the corresponding eigenvectors (i.e., helicity basis) $|s\mathbf{k}\rangle = a_{s\mathbf{k}}^\dagger|0\rangle$ can be represented as $|+, \mathbf{k}\rangle = (u_{\mathbf{k}} \quad v_{\mathbf{k}} e^{i\varphi_{\mathbf{k}}})^{\mathrm{T}}$ for the upper helicity band and $|-, \mathbf{k}\rangle = (-v_{\mathbf{k}} e^{-i\varphi_{\mathbf{k}}} \quad u_{\mathbf{k}})^{\mathrm{T}}$ for the lower helicity band, where $u_{\mathbf{k}} = \sqrt{(d_{\mathbf{k}} + d_{\mathbf{k}}^z)/(2d_{\mathbf{k}})}$, $v_{\mathbf{k}} = \sqrt{(d_{\mathbf{k}} - d_{\mathbf{k}}^z)/(2d_{\mathbf{k}})}$, $\varphi_{\mathbf{k}} = \arg(d_{\mathbf{k}}^x + i d_{\mathbf{k}}^y)$, and T denotes the transpose. Alternatively,

$$\begin{pmatrix} a_{\uparrow\mathbf{k}} \\ a_{\downarrow\mathbf{k}} \end{pmatrix} = \begin{pmatrix} u_{\mathbf{k}} & -v_{\mathbf{k}} e^{-i\varphi_{\mathbf{k}}} \\ v_{\mathbf{k}} e^{i\varphi_{\mathbf{k}}} & u_{\mathbf{k}} \end{pmatrix} \begin{pmatrix} a_{+,\mathbf{k}} \\ a_{-,\mathbf{k}} \end{pmatrix}$$

is the transformation between the annihilation operators for the pseudospin and helicity states.

For notational convenience, the lower helicity state $|-, \mathbf{k}\rangle$ is denoted as $|\phi_{\mathbf{k}}\rangle$ in the rest of the paper. Then the single-particle ground state $|\phi_{\mathbf{k}_0}\rangle$ is determined by setting $\partial\xi_{-,\mathbf{k}}/\partial k_i = 0$, leading to either $k_i = 0$ or $\alpha_i^2 = d_{\mathbf{k}}$. Here we choose $\mathbf{k_0} = (\alpha_x, 0, 0)$ without the loss of generality [18–20], for which case the single-particle ground-state energy $\xi_{-,\mathbf{k_0}} = 0$ vanishes (see Fig. 1) and the single-particle ground state $|\phi_{\mathbf{k}_0}\rangle = (-1/\sqrt{2} \quad 1/\sqrt{2})^{\mathrm{T}}$ admits a real representation. Note that the ground state is at least twofold degenerate with the opposite-momentum state $|\phi_{-\mathbf{k}_0}\rangle = (1/\sqrt{2} \quad 1/\sqrt{2})^{\mathrm{T}}$, and we highlight its competing role in Sec. III D. Having introduced the theoretical model and discussed its single-particle ground state, next we analyze the many-body ground state within the Bogoliubov mean-field approximation.

III. BOGOLIUBOV THEORY

Under the Bogoliubov mean-field approximation, the many-body ground state is known to be either a plane-wave condensate or a stripe phase depending on the relative strengths between the intraspin and interspin interactions [18–22]. See Sec. III D for a detailed account of the stability analysis. Assuming that $U_{\uparrow\downarrow}$ is sufficiently weak, here we concentrate only on the former phase.

A. Bogoliubov spectrum

In order to describe the many-body ground state $|\phi_{\mathbf{k}_0}\rangle$ that is macroscopically occupied by N_0 particles, we replace the annihilation and creation operators in accordance with $a_{\sigma\mathbf{k}} = \Delta_\sigma\sqrt{V}\delta_{\mathbf{k}\mathbf{k}_0} + \tilde{a}_{\sigma\mathbf{k}}$. Here the complex field $\Delta_\sigma = \sqrt{n_0}\langle\sigma|\phi_{\mathbf{k}_0}\rangle$ corresponds to the mean-field order parameter for the condensate with condensate density $n_0 = N_0/V$, δ_{ij} is a Kronecker delta, and the operator $\tilde{a}_{\sigma\mathbf{k}}$ denotes the fluctuations on top of the ground state. Following the usual recipe, we neglect the third- and fourth-order fluctuation terms in the interaction Hamiltonian. Then the excitations are described by the so-called Bogoliubov Hamiltonian

$$\mathcal{H}_\mathrm{B} = \frac{1}{2}\sum_{\mathbf{q}}{}' \Psi_{\mathbf{q}}^\dagger \begin{pmatrix} \mathbf{H}_{\mathbf{q}}^{pp} & \mathbf{H}_{\mathbf{q}}^{ph} \\ \mathbf{H}_{\mathbf{q}}^{hp} & \mathbf{H}_{\mathbf{q}}^{hh} \end{pmatrix} \Psi_{\mathbf{q}}, \tag{4}$$

$$\mathbf{H}_{\mathbf{q}}^{pp} = \begin{pmatrix} K_{\uparrow\mathbf{q}} & U_{\uparrow\downarrow}\Delta_\uparrow\Delta_\downarrow^* \\ U_{\uparrow\downarrow}\Delta_\uparrow^*\Delta_\downarrow & K_{\downarrow\mathbf{q}} \end{pmatrix} + \frac{\mathbf{d}_{\mathbf{k}_0+q}\cdot\boldsymbol{\sigma}}{m}, \tag{5}$$

$$\mathbf{H}_{\mathbf{q}}^{ph} = \begin{pmatrix} U_{\uparrow\uparrow}\Delta_\uparrow^2 & U_{\uparrow\downarrow}\Delta_\uparrow\Delta_\downarrow \\ U_{\uparrow\downarrow}\Delta_\uparrow\Delta_\downarrow & U_{\downarrow\downarrow}\Delta_\downarrow^2 \end{pmatrix}, \tag{6}$$

where $\Psi_{\mathbf{q}}^\dagger = (\tilde{a}_{\uparrow,\mathbf{k}_0+\mathbf{q}}^\dagger\ \tilde{a}_{\downarrow,\mathbf{k}_0+\mathbf{q}}^\dagger\ \tilde{a}_{\uparrow,\mathbf{k}_0-\mathbf{q}}\ \tilde{a}_{\downarrow,\mathbf{k}_0-\mathbf{q}})$ is a four-component spinor and $K_{\sigma\mathbf{q}} = \varepsilon_{\mathbf{k}_0+q} + \varepsilon_{\mathbf{k}_0} - \mu_\sigma + 2U_{\sigma\sigma}|\Delta_\sigma|^2 + U_{\uparrow\downarrow}|\Delta_{-\sigma}|^2$, with the index $-\sigma$ denoting the opposite component of the spin. The other terms are simply related via $\mathbf{H}_{\mathbf{q}}^{hh} = (\mathbf{H}_{-\mathbf{q}}^{pp})^*$ and $\mathbf{H}_{\mathbf{q}}^{hp} = (\mathbf{H}_{\mathbf{q}}^{ph})^\dagger$. The prime symbol indicates that the summation is over all of the noncondensed states. In this approximation, μ_σ is determined by setting the first-order fluctuation terms to zero, leading to $\mu_\sigma = U_{\sigma\sigma}|\Delta_\sigma|^2 + U_{\uparrow\downarrow}|\Delta_{-\sigma}|^2$. Note that $\Delta_\uparrow = -\Delta_\downarrow = -\sqrt{n_0/2}$ are real for our particular choice for the ground state $|\phi_{\mathbf{k}_0}\rangle$.

The Bogoliubov spectrum $E_{s\mathbf{q}}^n$ is determined by the eigenvalues of $\tau_z\mathbf{H}_{\mathbf{q}}$ [11,12], i.e.,

$$\tau_z\mathbf{H}_{\mathbf{q}}|\chi_{s\mathbf{q}}^n\rangle = E_{s\mathbf{q}}^n|\chi_{s\mathbf{q}}^n\rangle, \tag{7}$$

where τ_z is a Pauli matrix acting only on the particle-hole sector, $\mathbf{H}_{\mathbf{q}}$ is the 4×4 Hamiltonian matrix shown in Eq. (4), and $|\chi_{s\mathbf{q}}^n\rangle$ is the corresponding Bogoliubov state. Here $n=\pm$ label, respectively, the upper and lower Bogoliubov bands, and $s=\pm$ label, respectively, the quasiparticle and quasihole branches for a given band n, leading to four Bogoliubov modes for a given $\mathbf{q}$. The Bogoliubov states are normalized in the usual way; that is, if we denote $|\chi_{s\mathbf{q}}^n\rangle = \binom{|\chi_{s\mathbf{q}}^n\rangle_1}{|\chi_{s\mathbf{q}}^n\rangle_2}$, then ${}_1\langle\chi_{s\mathbf{q}}^n|\chi_{s\mathbf{q}}^n\rangle_1 - {}_2\langle\chi_{s\mathbf{q}}^n|\chi_{s\mathbf{q}}^n\rangle_2 = s$. While the Bogoliubov spectrum exhibits $E_{s\mathbf{q}}^n = -E_{-s,-\mathbf{q}}^n$ as a manifestation of the quasiparticle-quasihole symmetry, Eq. (7) does not allow for a closed-form analytic solution in general, and its characterization requires a fully numerical procedure.

In order to gain some analytical insight into the low-energy Bogoliubov modes, we assume that the energy gap between the lower and upper helicity bands near the ground state $|\phi_{\mathbf{k}_0}\rangle$ is much larger than the interaction energy. This occurs when the SOC energy scale is much stronger than the interaction energy scale. In this case the occupation of the upper band is negligible, and the system can be projected solely to the lower band as discussed next.

B. Projected system

The total Hamiltonian $\mathcal{H}$ of the system can be projected to the lower helicity band as follows [18]. Using the identity operator $\sigma_0 = \sum_s |s\mathbf{k}\rangle\langle s\mathbf{k}|$ for a given $\mathbf{k}$, we first reexpress $a_{\sigma\mathbf{k}} = \sum_s\langle\sigma|s\mathbf{k}\rangle a_{s\mathbf{k}}$ and discard those terms that involve the upper band, i.e., $a_{\sigma\mathbf{k}} \to \langle\sigma|\phi_{\mathbf{k}}\rangle a_{-,\mathbf{k}}$. This procedure leads to

$$h_0 + h_\mu = \sum_{\mathbf{k}}(\xi_{-,\mathbf{k}} - \mu)a_{-,\mathbf{k}}^\dagger a_{-,\mathbf{k}}, \tag{8}$$

$$h_U = \frac{1}{2V}\sum_{\mathbf{k}_1+\mathbf{k}_2=\mathbf{k}_3+\mathbf{k}_4} f_{\mathbf{k}_1\mathbf{k}_2}^{\mathbf{k}_3\mathbf{k}_4} a_{-,\mathbf{k}_1}^\dagger a_{-,\mathbf{k}_2}^\dagger a_{-,\mathbf{k}_3} a_{-,\mathbf{k}_4}, \tag{9}$$

$$f_{\mathbf{k}_1\mathbf{k}_2}^{\mathbf{k}_3\mathbf{k}_4} = \sum_{\sigma\sigma'} U_{\sigma\sigma'}\langle\phi_{\mathbf{k}_1}|\sigma\rangle\langle\phi_{\mathbf{k}_2}|\sigma'\rangle\langle\sigma'|\phi_{\mathbf{k}_3}\rangle\langle\sigma|\phi_{\mathbf{k}_4}\rangle, \tag{10}$$

where $\mu = (\mu_\uparrow + \mu_\downarrow)/2$ is the effective chemical potential and $f_{\mathbf{k}_1\mathbf{k}_2}^{\mathbf{k}_3\mathbf{k}_4} = U_{\uparrow\uparrow}v_{\mathbf{k}_1}v_{\mathbf{k}_2}v_{\mathbf{k}_3}v_{\mathbf{k}_4}e^{i(\varphi_{\mathbf{k}_1}+\varphi_{\mathbf{k}_2}-\varphi_{\mathbf{k}_3}-\varphi_{\mathbf{k}_4})} + U_{\downarrow\downarrow}u_{\mathbf{k}_1}u_{\mathbf{k}_2}u_{\mathbf{k}_3}u_{\mathbf{k}_4} + U_{\uparrow\downarrow}v_{\mathbf{k}_1}u_{\mathbf{k}_2}u_{\mathbf{k}_3}v_{\mathbf{k}_4}e^{i(\varphi_{\mathbf{k}_1}-\varphi_{\mathbf{k}_4})}$ is the effective long-range interaction for the projected system. We note that the long-range nature of the effective interaction plays a crucial role in the Bogoliubov spectrum as discussed in Sec. III D.

Under the Bogoliubov mean-field approximation that is used in Sec. III A, we replace the creation and annihilation operators in accordance with $a_{-,\mathbf{k}} = \sqrt{N_0}\delta_{\mathbf{k}\mathbf{k}_0} + \tilde{a}_{-,\mathbf{k}}$ and set the first-order fluctuation terms to zero. This leads to $\mu = n_0 f_{\mathbf{k}_0\mathbf{k}_0}^{\mathbf{k}_0\mathbf{k}_0} = (n_0/4)\sum_{\sigma\sigma'}U_{\sigma\sigma'}$, which is consistent with μ_σ found in Sec. III A. The zeroth-order fluctuation terms give $-\mu N_0 + n_0 f_{\mathbf{k}_0\mathbf{k}_0}^{\mathbf{k}_0\mathbf{k}_0}N_0/2$. Then the excitations above the ground state are described by the Bogoliubov Hamiltonian

$$h_\mathrm{B} = \frac{1}{2}\sum_{\mathbf{q}}{}' \psi_{\mathbf{q}}^\dagger \begin{pmatrix} h_{\mathbf{q}}^{pp} & h_{\mathbf{q}}^{ph} \\ h_{\mathbf{q}}^{hp} & h_{\mathbf{q}}^{hh} \end{pmatrix} \psi_{\mathbf{q}}, \tag{11}$$

$$h_{\mathbf{q}}^{pp} = \xi_{-,\mathbf{k}_0+\mathbf{q}} - \mu + \frac{n_0}{2}\big(f_{\mathbf{k}_0,\mathbf{k}_0+\mathbf{q}}^{\mathbf{k}_0,\mathbf{k}_0+\mathbf{q}} + f_{\mathbf{k}_0+\mathbf{q},\mathbf{k}_0}^{\mathbf{k}_0+\mathbf{q},\mathbf{k}_0} + f_{\mathbf{k}_0+\mathbf{q},\mathbf{k}_0}^{\mathbf{k}_0,\mathbf{k}_0+\mathbf{q}} + f_{\mathbf{k}_0,\mathbf{k}_0+\mathbf{q}}^{\mathbf{k}_0+\mathbf{q},\mathbf{k}_0}\big), \tag{12}$$

$$h_{\mathbf{q}}^{ph} = \frac{n_0}{2}\big(f_{\mathbf{k}_0+\mathbf{q},\mathbf{k}_0-\mathbf{q}}^{\mathbf{k}_0,\mathbf{k}_0} + f_{\mathbf{k}_0-\mathbf{q},\mathbf{k}_0+\mathbf{q}}^{\mathbf{k}_0,\mathbf{k}_0}\big), \tag{13}$$

where $\psi_{\mathbf{q}}^\dagger = (\tilde{a}_{-,\mathbf{k}_0+\mathbf{q}}^\dagger\ \tilde{a}_{-,\mathbf{k}_0-\mathbf{q}})$ is a two-component spinor and the other terms are simply related via $h_{\mathbf{q}}^{hh} = h_{-\mathbf{q}}^{pp}$ and $h_{\mathbf{q}}^{hp} = (h_{\mathbf{q}}^{ph})^*$. The Bogoliubov spectrum $\epsilon_{s\mathbf{q}}$ is determined by the eigenvalues of $\tau_z\mathbf{h}_{\mathbf{q}}$, leading to two Bogoliubov modes for a given $\mathbf{q}$, i.e.,

$$\epsilon_{s\mathbf{q}} = \frac{h_{\mathbf{q}}^{pp} - h_{\mathbf{q}}^{hh}}{2} + s\sqrt{\left(\frac{h_{\mathbf{q}}^{pp} + h_{\mathbf{q}}^{hh}}{2}\right)^2 - |h_{\mathbf{q}}^{ph}|^2}, \tag{14}$$

$$h_{\mathbf{q}}^{pp} = \xi_{-,\mathbf{k}_0+\mathbf{q}} - \mu + \frac{n_0}{2}\sum_{\sigma\sigma'}U_{\sigma\sigma'}|\langle\phi_{\mathbf{k}_0+q}|\sigma\rangle|^2 + n_0\sum_{\sigma\sigma'}U_{\sigma\sigma'}\langle\phi_{\mathbf{k}_0+q}|\sigma'\rangle\langle\sigma'|\phi_{\mathbf{k}_0}\rangle\langle\phi_{\mathbf{k}_0}|\sigma\rangle\langle\sigma|\phi_{\mathbf{k}_0+q}\rangle, \tag{15}$$

$$h_{\mathbf{q}}^{ph} = n_0\sum_{\sigma\sigma'}U_{\sigma\sigma'}\langle\phi_{\mathbf{k}_0+q}|\sigma\rangle\langle\sigma|\phi_{\mathbf{k}_0}\rangle\langle\phi_{\mathbf{k}_0}^*|\sigma'\rangle\langle\sigma'|\phi_{\mathbf{k}_0-q}^*\rangle. \tag{16}$$

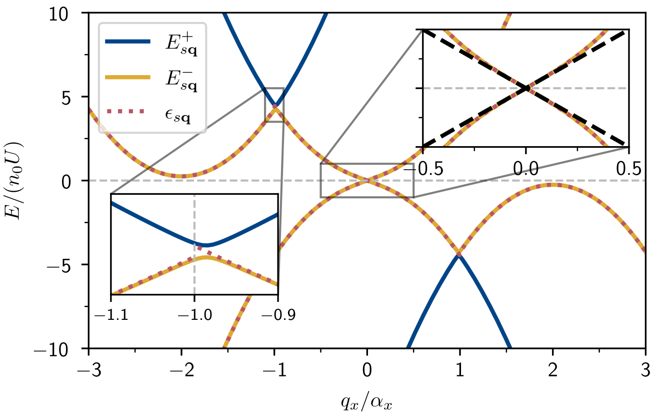

FIG. 2. The Bogoliubov spectrum is shown as a function of q_x when $q_y = 0 = q_z$, $U = U_{\uparrow\uparrow} = 2U_{\downarrow\downarrow} = 4U_{\uparrow\downarrow}$, $\alpha_x = \alpha_y = 2/\xi$ with the healing length $\xi = 1/\sqrt{2mnU}$ and $\alpha_z = 0$. Here the total particle density $n \approx n_0$ is set to $na^3 = 10^{-6}$, where $a = mU/(4\pi)$ is the scattering length. The full spectrum (solid lines) is shown together with the projected one (dotted lines) that is given by Eq. (14). In addition the low-q expansion (20) is shown as dashed black lines in the right inset. If one sets $U_{\uparrow\uparrow} = U_{\downarrow\downarrow}$, then the band gap shown in the left inset disappears; see Sec. III E for the analysis of the spurious jumps at $q_x = \mp\alpha_x$. If one sets $U_{\uparrow\downarrow} = U_{\uparrow\uparrow} = U_{\downarrow\downarrow}$, then two additional zero-energy modes appear at $q_x = \mp 2\alpha_x$; see Sec. III D for the analysis of the roton instability.

Here $s = \pm$ label, respectively, the quasiparticle and quasihole branches of the lower Bogoliubov band (i.e., $n = -$) discussed in Sec. III A. See Fig. 2 for their excellent numerical benchmark except for the spurious jumps at $\mathbf{q} = \mp\mathbf{k_0}$ that are discussed in Sec. III E. The Bogoliubov spectrum exhibits $\epsilon_{+,\mathbf{q}} = -\epsilon_{-,-\mathbf{q}}$ as a manifestation of the quasiparticle-quasihole symmetry. Note that when $U_{\sigma\sigma'} = U\delta_{\sigma\sigma'}$, these expressions reduce exactly to those of Refs. [11,12] with $M = 2$, where our $h^{pp}_{\mathbf{q}} = \xi_{-,\mathbf{k_0+q}} + Un_0/2$ and $h^{ph}_{\mathbf{q}}$ correspond, respectively, to their $\mathbf{q}^2/(2m_{\text{eff}}) + \mu$ and $\mu\alpha(\mathbf{q})$ provided that $\mu = Un_0/2$ in this particular case. Such a reduction may not be surprising since the intraspin interactions $U_{\uparrow\uparrow}$ and $U_{\downarrow\downarrow}$ play the roles of sublattice-dependent on-site interactions U_{AA} and U_{BB} and the interspin interaction $U_{\uparrow\downarrow}$ plays the role of a (long-range) intersublattice interaction U_{AB}. Thus, our $U_{\sigma\sigma'} = U\delta_{\sigma\sigma'}$ limit corresponds precisely to the $U = U_{AA} = U_{BB}$ and $U_{AB} = 0$ case that is considered in Refs. [11,12].

We can make further analytical progress through a low-$\mathbf{q}$ expansion around the ground state and use the fact that $|\langle\sigma|\phi_{\mathbf{k_0}}\rangle|^2 = 1/2$ for both pseudospin components; that is, the z component of $\mathbf{k_0}$ vanishes for the ground state.

C. Low-momentum expansion

Up to second order in $\mathbf{q}$, the low-energy expansions around the ground state $|\phi_{\mathbf{k_0}}\rangle$ can be written as

$$\begin{aligned} h^{pp}_{\mathbf{q}} =& \frac{1}{2}\sum_{ij} q_i q_j M^{-1}_{ij} - \mu + \frac{n_0}{2}\sum_{\sigma\sigma'} U_{\sigma\sigma'} + 2n_0 \sum_{i\sigma\sigma'} q_i U_{\sigma\sigma'} \\ & \times \text{Re}\langle\partial_i\phi_{\mathbf{k}}|\sigma\rangle\langle\sigma|\phi_{\mathbf{k_0}}\rangle + n_0 \sum_{ij\sigma\sigma'} q_i q_j U_{\sigma\sigma'} \\ & \times (\text{Re}\langle\partial_i\partial_j\phi_{\mathbf{k}}|\sigma\rangle\langle\sigma|\phi_{\mathbf{k_0}}\rangle + \langle\partial_i\phi_{\mathbf{k}}|\sigma\rangle\langle\sigma|\partial_j\phi_{\mathbf{k}}\rangle/2 \\ & + \langle\partial_i\phi_{\mathbf{k}}|\sigma'\rangle\langle\sigma'|\phi_{\mathbf{k_0}}\rangle\langle\phi_{\mathbf{k_0}}|\sigma\rangle\langle\sigma|\partial_j\phi_{\mathbf{k}}\rangle), \end{aligned} \quad (17)$$

$$\begin{aligned} h^{ph}_{\mathbf{q}} =& \frac{n_0}{4}\sum_{\sigma\sigma'} U_{\sigma\sigma'} + \frac{n_0}{2}\sum_{ij\sigma\sigma'} q_i q_j U_{\sigma\sigma'}(\langle\partial_i\partial_j\phi_{\mathbf{k}}|\sigma\rangle\langle\sigma|\phi_{\mathbf{k_0}}\rangle \\ & - 2\langle\partial_i\phi_{\mathbf{k}}|\sigma\rangle\langle\sigma|\phi_{\mathbf{k_0}}\rangle\langle\phi^*_{\mathbf{k_0}}|\sigma'\rangle\langle\sigma'|\partial_j\phi^*_{\mathbf{k}}\rangle), \end{aligned} \quad (18)$$

where the spectrum of the lower helicity band is expanded as $\xi_{-,\mathbf{k_0+q}} = (1/2)\sum_{ij} q_i q_j M^{-1}_{ij}$. Here $\mathbf{M}^{-1}$ is the inverse of the effective-mass tensor whose elements are given by $M^{-1}_{xx} = 1/m$, $M^{-1}_{yy} = 1/m - \alpha_y^2/(m\alpha_x^2)$, and $M^{-1}_{zz} = 1/m - \alpha_z^2/(m\alpha_x^2)$ and are zero otherwise. In addition Re denotes the real part of an expression, and $|\partial_i\phi_{\mathbf{k}}\rangle$ stands for $\partial|\phi_{\mathbf{k}}\rangle/\partial k_i$ in the $\mathbf{k} \to \mathbf{k_0}$ limit. By plugging these expansions in Eq. (14) and keeping up to second-order terms in $\mathbf{q}$, we obtain

$$\epsilon_{s\mathbf{q}} = 2n_0 \sum_{i\sigma\sigma'} q_i U_{\sigma\sigma'}\text{Re}\langle\partial_i\phi_{\mathbf{k}}|\sigma\rangle\langle\sigma|\phi_{\mathbf{k_0}}\rangle + s\sqrt{X_{\mathbf{q}}},$$

$$\begin{aligned} X_{\mathbf{q}} =& \mu\sum_{ij} q_i q_j \Big[M^{-1}_{ij} + n_0\sum_{\sigma\sigma'} U_{\sigma\sigma'}(\langle\partial_i\phi_{\mathbf{k}}|\sigma\rangle\langle\sigma|\partial_j\phi_{\mathbf{k}}\rangle \\ & + \text{Re}\langle\partial_i\partial_j\phi_{\mathbf{k}}|\sigma\rangle\langle\sigma|\phi_{\mathbf{k_0}}\rangle + 2\langle\partial_i\phi_{\mathbf{k}}|\sigma'\rangle\langle\sigma'|\phi_{\mathbf{k_0}}\rangle\langle\phi_{\mathbf{k_0}}|\sigma\rangle \\ & \times\langle\sigma|\partial_j\phi_{\mathbf{k}}\rangle + 2\text{Re}\langle\partial_i\phi_{\mathbf{k}}|\sigma'\rangle\langle\sigma'|\phi_{\mathbf{k_0}}\rangle\langle\phi^*_{\mathbf{k_0}}|\sigma\rangle\langle\sigma|\partial_j\phi^*_{\mathbf{k}}\rangle)\Big] \end{aligned} \quad (19)$$

for the low-energy Bogoliubov spectrum of the projected system. In addition to the conventional effective-mass term that depends only on the helicity spectrum, here we have the so-called geometric terms that depend also on the helicity states. The quantum geometry of the underlying Hilbert space is masked by those terms that depend on $|\partial_i\phi_{\mathbf{k}}\rangle$ and $|\partial_i\partial_j\phi_{\mathbf{k}}\rangle$ [11,12]. While most of these terms cancel one another, they lead to

$$\begin{aligned} \epsilon_{s\mathbf{q}} =& n_0(U_{\downarrow\downarrow} - U_{\uparrow\uparrow})\frac{\alpha_z q_z}{2\alpha_x^2} + \frac{s}{2}\sqrt{n_0(U_{\uparrow\uparrow} + U_{\downarrow\downarrow} + 2U_{\uparrow\downarrow})} \\ & \times\sqrt{\sum_{ij} q_i q_j M^{-1}_{ij} + n_0(U_{\uparrow\uparrow} + U_{\downarrow\downarrow} - 2U_{\uparrow\downarrow})\frac{\alpha_z^2 q_z^2}{4\alpha_x^4}}, \end{aligned} \quad (20)$$

manifesting explicitly the quasiparticle-quasihole symmetry. When $U_{\uparrow\uparrow} = U_{\downarrow\downarrow}$, Eq. (20) is in full agreement with the recent literature on the reported parameters [18]. In addition see the right inset in Fig. 2 for its numerical benchmark with Eq. (14).

Our work reveals that the linear term in $\alpha_z q_z$ that is outside of the square root and the quadratic term in $\alpha_z q_z$ that is in inside it have a quantum-geometric origin. Note that the geometric terms that depend on α_x and α_y vanish altogether. Thus, we conclude that the geometric effects survive only in the presence of a finite σ_z coupling assuming a σ_x (and/or, equivalently, a σ_y) coupling to begin with. See Sec. II B for our initial assumption in choosing $\mathbf{k_0}$. Although we choose a $\mathbf{k_0}$ that is symmetric in the y and z directions, the condition $|\langle\sigma|\phi_{\mathbf{k_0}}\rangle|^2 = 1/2$ breaks this symmetry in general for other $\mathbf{k_0}$ values as it requires $k_{0z} = 0$. The remaining geometric terms can be isolated from the conventional effective-mass term in the $\mathbf{q} \to (0, 0, q_z)$ limit when $\alpha_z \approx \alpha_x$, leading to

$q_i q_j M_{ij}^{-1} = 0$. Therefore, this particular limit can be used to distinguish the geometric origin of the sound velocity from the conventional one; that is, unlike the conventional term that has $\propto \sqrt{U}$ dependence on the interaction strength, the geometric ones have $\propto U$ dependence. The square-root vs linear dependence is consistent with the recent results on multiband Bloch systems [11,12]. We note that the geometric term that is inside the square root can be incorporated into the conventional effective-mass term, leading to a "dressed" effective mass $M_{zz}^{-1} \to M_{zz}^{-1} + n_0(U_{\uparrow\uparrow} + U_{\downarrow\downarrow} - 2U_{\uparrow\downarrow})\alpha_z^2/(4\alpha_x^4)$ for the Bogoliubov modes [11,12]. While this geometric dressing shares some similarities with the dressing of the effective-mass tensor of the Cooper pairs or the Goldstone modes in spin-orbit-coupled Fermi SFs, their mathematical structures are entirely different [4,5]. The latter involves a **k**-space sum over the quantum-metric tensor of the helicity bands that is weighted by a function of other quantities, including the excitation spectrum.

We note in passing that when $U_{\sigma\sigma'} = U\delta_{\sigma\sigma'}$, our Eq. (19) reduces exactly to that of Refs. [11,12] with $M = 2$, for which case we obtain $\epsilon_{s\mathbf{q}} = s\epsilon_{\mathbf{q}}$, with $\epsilon_{\mathbf{q}} = [(Un_0/2)\sum_{ij} q_i q_j (M_{ij}^{-1} + Un_0\langle\partial_i\phi_{\mathbf{k}}|\partial_j\phi_{\mathbf{k}}\rangle + 2Un_0\sum_\sigma \mathrm{Re}\langle\partial_i\phi_{\mathbf{k}}|\sigma\rangle\langle\sigma|\phi_{\mathbf{k}_0}\rangle\langle\phi_{\mathbf{k}_0}^*|\sigma\rangle\langle\sigma|\partial_j\phi_{\mathbf{k}}^*\rangle)]^{1/2}$. Furthermore, using the fact that $|\phi_{\mathbf{k}_0}\rangle$ is real for the ground state, we find $\epsilon_{\mathbf{q}} = [(Un_0/2)\sum_{ij} q_i q_j (M_{ij}^{-1} + Un_0\langle\partial_i\phi_{\mathbf{k}}|\partial_j\phi_{\mathbf{k}}\rangle + Un_0\mathrm{Re}\langle\partial_i\phi_{\mathbf{k}}|\partial_j\phi_{\mathbf{k}}^*\rangle)]^{\frac{1}{2}}$. In comparison the quantum metric of the lower helicity band is defined by $g_{ij}^{\mathbf{k}} = \mathrm{Re}\langle\partial_i\phi_{\mathbf{k}}|(\sigma_0 - |\phi_{\mathbf{k}}\rangle\langle\phi_{\mathbf{k}}|)|\partial_j\phi_{\mathbf{k}}\rangle$, and it reduces to $g_{ij}^{\mathbf{k}} = \langle\partial_i\phi_{\mathbf{k}}|\partial_j\phi_{\mathbf{k}}\rangle$ only when $|\phi_{\mathbf{k}}\rangle$ is real for all **k**. This is because $\langle\partial_i\phi_{\mathbf{k}}|\phi_{\mathbf{k}}\rangle = -\langle\phi_{\mathbf{k}}|\partial_i\phi_{\mathbf{k}}\rangle = -\langle\partial_i\phi_{\mathbf{k}}^*|\phi_{\mathbf{k}}^*\rangle$ must vanish when $\phi_{\mathbf{k}}$ is real. Thus, we conclude that the geometric dressing of the effective mass of the Bogoliubov modes can be written in terms of $g_{ij}^{\mathbf{k}}$ when $|\phi_{\mathbf{k}}\rangle$ is real for all **k**. This is clearly the case when $d_{\mathbf{k}}^y = 0$ in two-band lattices and when $\alpha_y = 0$ in spin-orbit-coupled Bose SFs.

Furthermore, when $\alpha_z \neq 0$, we find that the competition between the linear term in q_z that is outside of the square root and the quadratic terms within the square root in Eq. (20) causes an energetic instability (i.e., $\epsilon_{s\mathbf{q}}$ changes sign and becomes $\epsilon_{\pm,\mathbf{q}\lessgtr 0}$) in the $\mathbf{q} \to \mathbf{0}$ limit unless

$$\frac{4U_{\uparrow\downarrow}^2 - (3U_{\uparrow\uparrow} - U_{\downarrow\downarrow})(3U_{\downarrow\downarrow} - U_{\uparrow\uparrow})}{U_{\uparrow\uparrow} + U_{\downarrow\downarrow} + 2U_{\uparrow\downarrow}} \leqslant \frac{4\alpha_x^2}{mn_0}\left(\frac{\alpha_x^2}{\alpha_z^2} - 1\right) \tag{21}$$

is satisfied. For instance, this condition reduces to $3U_{\downarrow\downarrow} \geqslant U_{\uparrow\uparrow} \geqslant U_{\downarrow\downarrow}/3$ when $\alpha_z = \alpha_x$ in the $U_{\uparrow\downarrow} \to 0$ limit, revealing a peculiar constraint on the strength of the interactions. Our calculation suggests that the physical origin of this instability is related to the quantum geometry of the underlying space without deeper insight. In addition, when $\alpha_z \neq 0$, Eq. (20) further suggests that there is a dynamical instability (i.e., $\epsilon_{s\mathbf{q}}$ becomes complex) unless the quadratic terms within the square root are positive, i.e., $1 - \alpha_z^2/\alpha_x^2 + mn_0\alpha_z^2(U_{\uparrow\uparrow} + U_{\downarrow\downarrow} - 2U_{\uparrow\downarrow})/(4\alpha_x^4) \geqslant 0$. This condition is most restrictive when $\alpha_z \to \alpha_x$, giving rise to $(U_{\uparrow\uparrow} + U_{\downarrow\downarrow})/2 \geqslant U_{\uparrow\downarrow}$ for the dynamical stability of the system. Next, we show that the dynamical instability never takes place because it is preceded by the so-called roton instability, given that the geometric mean of $U_{\uparrow\uparrow}$ and $U_{\downarrow\downarrow}$ is guaranteed to be less than or equal to the arithmetic mean.

D. Roton instability at $\mathbf{q} = \mp 2\mathbf{k_0}$

The zero-energy Bogoliubov mode that is found at $\mathbf{q} = \mathbf{0}$ is a special example of the Goldstone mode that is associated with the spontaneous breaking of continuous symmetry in SF systems. In addition to this phonon mode, the Bogoliubov spectrum also exhibits the so-called roton mode at finite **q**. This peculiar spectrum clearly originates from the long-range interaction characterized by Eq. (10), and it is a remarkable feature given the surge of recent interest in rotonlike spectra in various other cold-atom contexts [23–27] that paved the way for the creation of dipolar Bose supersolids [26,27]. Furthermore, the roton spectrum [28,29] along with some supersolid properties [30,31] has also been measured with Raman SOC. As a consequence of this outstanding progress, the roton spectrum is nowadays considered a possible route and precursor to the solidification of Bose SFs.

Depending on the interaction parameters, our numerics show that an additional pair of zero-energy modes at finite **q** may appear when the roton gap vanishes. See also Refs. [15,17,19,20,22,32] for related observations. It turns out they always appear precisely at opposite momenta $\mathbf{q} = \mp 2\mathbf{k_0}$ when the local minimum (maximum) of $\epsilon_{\pm,\mathbf{q}}$ touches the zero-energy axis with a quadratic dispersion away from it. For instance, the roton minimum and its gap are clearly visible in Fig. 2 at $q_x = \mp 2\alpha_x$.

Given this numerical observation, we evaluate Eqs. (15) and (16) at $\mathbf{q} = \mp 2\mathbf{k_0}$, leading to, e.g., the quasiparticle-quasiparticle element $h_{-2\mathbf{k_0}}^{pp} = (U_{\uparrow\uparrow} + U_{\downarrow\downarrow} - 2U_{\uparrow\downarrow})n_0/4$, quasihole-quasihole element $h_{-2\mathbf{k_0}}^{hh} = \varepsilon_{3\mathbf{k_0}} + (U_{\uparrow\uparrow} + U_{\downarrow\downarrow} + 2U_{\uparrow\downarrow})n_0/4$, and quasiparticle-quasihole element $h_{-2\mathbf{k_0}}^{ph} = (U_{\downarrow\downarrow} - U_{\uparrow\uparrow})n_0/4$. Then, by plugging them into Eq. (14) and noting that the stability of the Bogoliubov theory requires the local minimum (maximum) of the quasiparticle (quasihole) spectrum to satisfy $\epsilon_{\pm,\mp 2\mathbf{k_0}} \gtrless 0$, we obtain the following condition:

$$\left(\frac{2\alpha_x^2}{mn_0} + U_{\uparrow\uparrow}\right)\left(\frac{2\alpha_x^2}{mn_0} + U_{\downarrow\downarrow}\right) > \left(\frac{2\alpha_x^2}{mn_0} + U_{\uparrow\downarrow}\right)^2. \tag{22}$$

This condition guarantees the energetic stability of the many-body ground state that is presumed in Sec. II B, and it is in full agreement with the previously known results. For instance, it reduces to $\sqrt{U_{\uparrow\uparrow}U_{\downarrow\downarrow}} > U_{\uparrow\downarrow}$ in the absence of SOC when $\alpha_x = 0$, and it reduces to $U > U_{\uparrow\downarrow}$ for equal intraspin interactions $U_{\uparrow\uparrow} = U_{\downarrow\downarrow} = U$ when $\alpha_x \neq 0$ [18,21]. In general Eq. (22) suggests that while the ground state is energetically stable for all α_x values when $\sqrt{U_{\uparrow\uparrow}U_{\downarrow\downarrow}} > U_{\uparrow\downarrow}$, it is stable for sufficiently strong SOC strengths $\alpha_x > \alpha_c$ when $\sqrt{U_{\uparrow\uparrow}U_{\downarrow\downarrow}} < U_{\uparrow\downarrow} < (U_{\uparrow\uparrow} + U_{\downarrow\downarrow})/2$. Here $\alpha_c = [mn_0(U_{\uparrow\downarrow}^2 - U_{\uparrow\uparrow}U_{\downarrow\downarrow})/(2U_{\uparrow\uparrow} + 2U_{\downarrow\downarrow} - 4U_{\uparrow\downarrow})]^{1/2}$ is the critical threshold.

Both the appearance of an additional pair of zero-energy modes at $\mathbf{q} = \mp 2\mathbf{k_0}$ and the associated instability of the many-body ground state that is caused by $\epsilon_{\pm,\mathbf{q}} \lessgtr 0$ can be traced back to the degeneracy of the lower helicity band $\xi_{-,\mathbf{k}}$ discussed in Sec. II B. For instance, when $\alpha_x \geqslant \{\alpha_y, \alpha_z\}$, our single-particle ground state $|\phi_{\mathbf{k_0}}\rangle$ is at least twofold degenerate with the opposite-momentum state $|\phi_{-\mathbf{k_0}}\rangle$. Note that the relative momentum between these two particle (hole) states is exactly $\mp 2\mathbf{k_0}$. Then Eq. (22) suggests that while our initial choice for a plane-wave condensate that is described purely by the state $|\phi_{\mathbf{k_0}}\rangle$ is energetically stable for sufficiently weak $U_{\uparrow\downarrow}$, it eventually becomes unstable against competing states with increasing $U_{\uparrow\downarrow}$. Since this instability also occurs precisely at $\mathbf{q} = \mp 2\mathbf{k_0}$, it clearly signals the possibility of an additional condensate that is described by the state $|\phi_{-\mathbf{k_0}}\rangle$. Thus, when Eq. (22) is not satisfied, we conclude that the many-body ground state corresponds to the so-called stripe phase that is described by a superposition of two states with opposite momenta, i.e., $|\phi_{\mathbf{k_0}}\rangle$ and $|\phi_{-\mathbf{k_0}}\rangle$ [15–17,21,22,32]. Indeed, some supersolid properties of the stripe phase have already been observed with Raman SOC [30,31].

We would like to emphasize that this conclusion is immune to the increased degeneracy of the helicity states when the SOC field is isotropic in momentum space. For instance, despite the circular degeneracy caused by a Rashba SOC when $\alpha_x = \alpha_y$, the zero-energy modes still appear at $\mathbf{q} = \mp 2\mathbf{k_0}$, and therefore, the stripe phase again involves a superposition of two states with opposite momenta.

E. Spurious jumps at $\mathbf{q} = \mp \mathbf{k_0}$

As shown in Fig. 2, there is an almost perfect agreement between the Bogoliubov spectrum of the 4×4 Hamiltonian and that of the 2×2 projected one except for a tiny region in the vicinity of a peculiar jump at $\mathbf{q} = \mp \mathbf{k_0}$. In order to reveal its physical origin, here we set $\alpha_z = 0$ for its simplicity and expand the Hamiltonian matrix at $\mathbf{q} = -\mathbf{k_0} + \boldsymbol{\delta}$ for a small $\boldsymbol{\delta} = (\delta, 0, 0)$. We find that

$$h_\delta^{pp} = \xi_{-,\delta} + \frac{n_0}{4}[U_{\uparrow\uparrow} + U_{\downarrow\downarrow} + 2U_{\uparrow\downarrow}\cos(\varphi_\delta)],$$

$$h_\delta^{ph} = \frac{n_0}{4}[U_{\uparrow\uparrow} - U_{\downarrow\downarrow} + 2U_{\uparrow\downarrow}\cos(\varphi_\delta)],$$

where the phase angle $\varphi_{\mathbf{k}}$ was defined in Sec. II B, leading to $\cos(\varphi_\delta) = \mathrm{sgn}(\delta)$. This analysis shows it is those coupling terms $U_{\uparrow\downarrow}\cos(\varphi_\delta)$ between the $\uparrow$ and $\downarrow$ sectors in the Bogoliubov Hamiltonian that are responsible for the spurious jump at $\delta = 0$ upon the change in sign of δ. Note that our initial motivation in deriving the projected Hamiltonian in Sec. III A is the assumption that the energy gap between the lower and upper helicity bands near the single-particle ground state $|\phi_{\mathbf{k_0}}\rangle$ is much larger than the interaction energy. While the validity region of this assumption in $\mathbf{k}$ space is not limited to the ground state, it clearly breaks down in the vicinity of $\mathbf{k} = \mathbf{0}$, where the $s = \pm$ helicity bands are degenerate (see Fig. 1). For this reason our projected Hamiltonian becomes unphysical and fails to capture the actual result in a tiny region around $\mathbf{q} = -\mathbf{k_0}$.

Having presented a detailed analysis of the Bogoliubov spectrum, next we determine the SF density tensor and compare it to the condensate density of the system.

IV. SUPERFLUID VERSUS CONDENSATE DENSITY

In this paper we define the SF density ρ_s by imposing a so-called phase twist on the mean-field order parameter [33–36]. When the SF flows uniformly with the momentum $\mathbf{Q}$, the SF order parameter transforms as $\Delta_\sigma \to \Delta_\sigma e^{i\mathbf{Q}\cdot\mathbf{r}}$, and the SF density tensor ρ_{ij} is defined as the response of the thermodynamic potential $\Omega_{\mathbf{Q}}$ to an infinitesimal flow, i.e.,

$$\rho_{ij} = \frac{m}{V}\lim_{\mathbf{Q}\to\mathbf{0}}\frac{\partial^2\Omega_{\mathbf{Q}}}{\partial Q_i \partial Q_j}. \tag{23}$$

Here the derivatives are taken for a constant Δ_σ and μ_σ; that is, the mean-field parameters do not depend on $\mathbf{Q}$ in the $\mathbf{Q} \to \mathbf{0}$ limit. We note that the SF mass-density tensor $m\rho_{ij}$ is a related quantity, and it corresponds to the total mass involved in the flow.

Let us now calculate $\Omega_{\mathbf{Q}}$ in the low-$\mathbf{Q}$ limit. In the absence of an SF flow when $\mathbf{Q} = \mathbf{0}$, the thermodynamic potential $\Omega_{\mathbf{0}}$ can be written as $\Omega_{\mathbf{0}} = \Omega_{zp} + (T/2)\sum_{\ell\mathbf{q}}' \mathrm{Tr}\ln \mathbf{G}_{\mathbf{0}\ell\mathbf{q}}^{-1}$, where $\Omega_{zp} = -\mu N_0/2 - \sum_{\mathbf{q}}' (\varepsilon_{\mathbf{q}} + \mu)/2$ is the zero-point contribution, T is the temperature with the Boltzmann constant $k_B = 1$, Tr is the trace, and $\mathbf{G}_{\mathbf{0}\ell\mathbf{q}}^{-1} = i\omega_\ell\sigma_0\tau_z - \mathbf{H}_{\mathbf{q}}$ is the inverse of the Green's function for the Bogoliubov Hamiltonian that is given in Eq. (4). Here $\omega_\ell = 2\pi\ell T$ is the bosonic Matsubara frequency, with ℓ being an integer. In order to make some analytical progress, we make use of the Bogoliubov states and spectrum determined by Eq. (7) and define [11,12]

$$\mathbf{G}_{\mathbf{0}\ell\mathbf{q}} = \sum_{ns}\frac{s|\chi_{s\mathbf{q}}^n\rangle\langle\chi_{s\mathbf{q}}^n|}{i\omega_\ell - E_{s\mathbf{q}}^n}. \tag{24}$$

This expression clearly satisfies $\mathbf{G}_{\mathbf{0}\ell\mathbf{q}}^{-1}\mathbf{G}_{\mathbf{0}\ell\mathbf{q}} = \sigma_0\tau_0$. In the presence of an SF flow when $\mathbf{Q} \neq \mathbf{0}$, the thermodynamic potential $\Omega_{\mathbf{Q}}$ can be obtained through a gauge transformation of the bosonic field operators $\tilde{a}_{\sigma\mathbf{q}} \to \tilde{a}_{\sigma\mathbf{q}}e^{i\mathbf{Q}\cdot\mathbf{r}}$. This transformation removes the phases of the SF order parameters, and we obtain the inverse Green's function $\mathbf{G}_{\mathbf{Q}\ell\mathbf{q}}^{-1} = \mathbf{G}_{\mathbf{0}\ell\mathbf{q}}^{-1} - \mathbf{\Sigma}_{\mathbf{Q}}$ of the twisted system. Its $\mathbf{Q}$-dependent part has three terms, $\mathbf{\Sigma}_{\mathbf{Q}} = \mathbf{\Sigma}_{\mathbf{Q},1} + \mathbf{\Sigma}_{\mathbf{Q},2} + \mathbf{\Sigma}_{\mathbf{Q},3}$ [36]: while the SOC-independent terms $\mathbf{\Sigma}_{\mathbf{Q},1} = \frac{Q^2}{2m}\sigma_0\tau_0$ and

$$\mathbf{\Sigma}_{\mathbf{Q},2} = \frac{\sigma_0}{m}\begin{bmatrix}(\mathbf{k_0}+\mathbf{q})\cdot\mathbf{Q} & 0\\ 0 & (\mathbf{k_0}-\mathbf{q})\cdot\mathbf{Q}\end{bmatrix}$$

are diagonal in both the spin and particle-hole sectors, the SOC-induced term

$$\mathbf{\Sigma}_{\mathbf{Q},3} = \frac{1}{m}\begin{pmatrix}\mathbf{d_Q}\cdot\boldsymbol{\sigma} & 0\\ 0 & \mathbf{d_Q}\cdot\boldsymbol{\sigma}^*\end{pmatrix}$$

is diagonal only in the particle-hole sector. These terms can be conveniently reexpressed as $\mathbf{\Sigma}_{\mathbf{Q},1} = (1/2)\sum_{ij} Q_iQ_j\partial_i\partial_j\mathbf{H}_{\mathbf{q}}$ and $\mathbf{\Sigma}_{\mathbf{Q},2+3} = \sum_i Q_i\tau_z\partial_i\mathbf{H}_{\mathbf{q}}$, where $\partial_i\mathbf{H}_{\mathbf{q}}$ stands for $\partial\mathbf{H}_{\mathbf{q}}/\partial q_i$.

Since we are interested only in the low-$\mathbf{Q}$ limit of $\Omega_{\mathbf{Q}}$, we can use the Taylor expansion $\ln\det\mathbf{G}_{\mathbf{Q}\ell\mathbf{q}}^{-1} = \mathrm{Tr}\ln\mathbf{G}_{\mathbf{0}\ell\mathbf{q}}^{-1} - \mathrm{Tr}\sum_{l=1}^{\infty}(\mathbf{G}_{\mathbf{0}\ell\mathbf{q}}\mathbf{\Sigma}_{\mathbf{Q}})^l/l$, and keep up to second-order terms in $\mathbf{\Sigma}_{\mathbf{Q}}$. This calculation leads to

$$\rho_{ij} = mn_0M_{ij}^{-1} - \frac{mT}{2V}\sum_{\ell\mathbf{q}}'[\mathrm{Tr}(\mathbf{G}_{\mathbf{0}\ell\mathbf{q}}\partial_i\partial_j\mathbf{H}_{\mathbf{q}}) + \mathrm{Tr}(\mathbf{G}_{\mathbf{0}\ell\mathbf{q}}\tau_z\partial_i\mathbf{H}_{\mathbf{q}}\mathbf{G}_{\mathbf{0}\ell\mathbf{q}}\tau_z\partial_j\mathbf{H}_{\mathbf{q}})]. \tag{25}$$

Here the first term is due to the kinetic energy of the condensate in the presence of an SF flow; that is, there is an

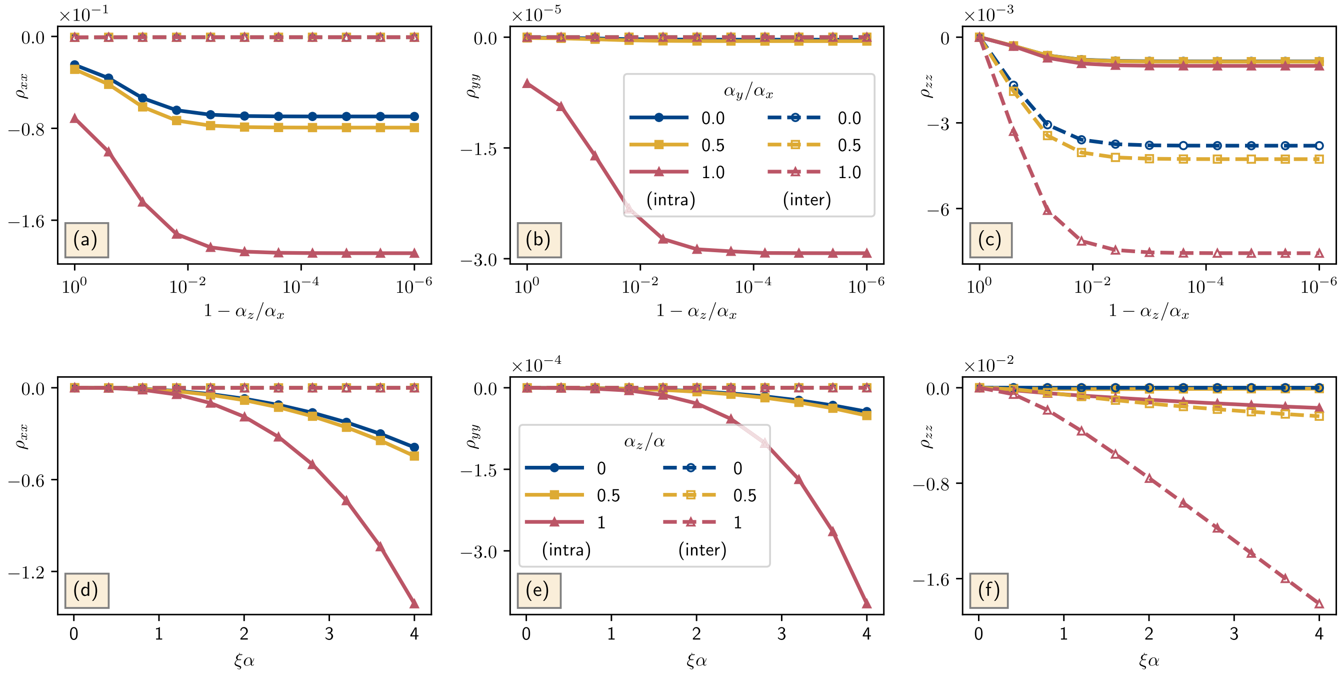

FIG. 3. The intraband (solid lines) and interband (dashed lines) contributions to the summation term in the superfluid-density tensor ρ_{ij} are shown when $T=0$ and $U=U_{\uparrow\uparrow}=U_{\downarrow\downarrow}=10U_{\uparrow\downarrow}/9$. Here the left, middle, and right columns correspond, respectively, to the diagonal elements ρ_{xx}, ρ_{yy}, and ρ_{zz} (in units of $n_0\approx n$), and all of the off-diagonal elements vanish. In the top row the diagonal elements are shown as a function of α_z for three values of α_y when $\alpha_x=2/\xi$ is fixed. In the bottom row the diagonal elements are shown as a function of the SOC strength $\alpha=\alpha_x=\alpha_y$ for three values of the α_z/α ratio.

additional quadratic contribution $(N_0/2)\sum_{ij}Q_iQ_jM_{ij}^{-1}$ to Ω_{zp} coming from the low-**Q** expansion of $\sum_{\mathbf{k}}\xi_{-,\mathbf{k}+\mathbf{Q}}a_{-,\mathbf{k}}^\dagger a_{-,\mathbf{k}}$ around $\mathbf{k_0}$. Thus, when the inverse of the effective-mass tensor M_{ij}^{-1} vanishes, ρ_{ij} is determined entirely by the Bogoliubov Hamiltonian, i.e., the quantum fluctuations above the condensate. The trace of the Green's function in the second term is related to the density of excited (noncondensate) particles n_e since its diagonal elements yield $n_e=-(T/V)\sum_{\ell\mathbf{q}}'(G_{\mathbf{0}\ell\mathbf{q}}^{11}+G_{\mathbf{0}\ell\mathbf{q}}^{22})e^{-i\omega_\ell 0^+}$, or, alternatively, $n_e=-(T/V)\sum_{\ell\mathbf{q}}'(G_{\mathbf{0}\ell\mathbf{q}}^{33}+G_{\mathbf{0}\ell\mathbf{q}}^{44})e^{i\omega_\ell 0^+}$. Thus, by performing the summation over the Matsubara frequencies, we eventually obtain

$$\rho_{ij}=n_t\delta_{ij}-n_0\frac{\alpha_y^2\delta_{iy}+\alpha_z^2\delta_{iz}}{\alpha_x^2}+\frac{m}{2V}\sum_{nn'ss'\mathbf{q}}{}' ss'\langle\chi_{s\mathbf{q}}^n|\tau_z\partial_i\mathbf{H}_\mathbf{q}|\chi_{s'\mathbf{q}}^{n'}\rangle\langle\chi_{s'\mathbf{q}}^{n'}|\tau_z\partial_j\mathbf{H}_\mathbf{q}|\chi_{s\mathbf{q}}^n\rangle\frac{f_\mathrm{B}(E_{s\mathbf{q}}^n)-f_\mathrm{B}(E_{s'\mathbf{q}}^{n'})}{E_{s\mathbf{q}}^n-E_{s'\mathbf{q}}^{n'}}, \tag{26}$$

where $n_t=n_0+n_e$ is the total density of particles in the system and $f_\mathrm{B}(x)$ is the Bose-Einstein distribution function. Here the partial derivative $\partial f_\mathrm{B}(E_{s\mathbf{q}}^n)/\partial E_{s\mathbf{q}}^n=-[1/(4T)]\mathrm{cosech}^2[E_{s\mathbf{q}}^n/(2T)]$ is implied when the summation indices coincide simultaneously ($n=n'$ and $s=s'$). In comparison to the SF density, the noncondensate density can be written as

$$n_\mathrm{e}=\frac{1}{2V}\sum_{ns\mathbf{q}}{}' s\big[\langle\chi_{s\mathbf{q}}^n|\chi_{s\mathbf{q}}^n\rangle f_\mathrm{B}(E_{s\mathbf{q}}^n)+{}_2\langle\chi_{s\mathbf{q}}^n|\chi_{s\mathbf{q}}^n\rangle_2\big] \tag{27}$$

$$=\frac{1}{2V}\sum_{ns\mathbf{q}}{}'\big[s\langle\chi_{s\mathbf{q}}^n|\chi_{s\mathbf{q}}^n\rangle f_\mathrm{B}(E_{s\mathbf{q}}^n)-1/2\big]. \tag{28}$$

We checked that both expressions yield the same numerical result. Note that $n_\mathrm{e}^0=[1/(2V)]\sum_{n\mathbf{q}}'(-1+\langle\chi_{-,\mathbf{q}}^n|\chi_{-,\mathbf{q}}^n\rangle)$ is the so-called quantum depletion of the condensate at $T=0$.

As an illustration, in the case of a single-component Bose gas, there is a single Bogoliubov band with the usual quasiparticle-quasihole symmetric spectrum $E_{s\mathbf{q}}=sE_\mathbf{q}$, where $E_\mathbf{q}=\sqrt{\varepsilon_\mathbf{q}(\varepsilon_\mathbf{q}+2Un_0)}$, and by plugging $\langle\chi_{s\mathbf{q}}|\tau_z\partial_i\mathbf{H}_\mathbf{q}|\chi_{s'\mathbf{q}}\rangle=(sq_i/m)\delta_{ss'}$ into Eq. (26), we recover the textbook definition $\rho_{ij}=n_t\delta_{ij}+[1/(mV)]\sum_\mathbf{q}'q_iq_j\partial f_\mathrm{B}(E_\mathbf{q})/\partial E_\mathbf{q}$ of ρ_s [37]. This shows that $\rho_{ij}=n_t\delta_{ij}$ at zero temperature and that the entire gas is SF. Similarly, by plugging $\langle\chi_{s\mathbf{q}}|\chi_{s'\mathbf{q}}\rangle=(\varepsilon_\mathbf{q}+Un_0)/E_\mathbf{q}$ into Eq. (28), we recover the textbook definition of $n_e=n_e^0+n_e^T$, where $n_e^0=[1/(2V)]\sum_\mathbf{q}'[-1+(\varepsilon_\mathbf{q}+Un_0)/E_\mathbf{q}]$ is the quantum depletion and $n_e^T=(1/V)\sum_\mathbf{q}'(\varepsilon_\mathbf{q}+Un_0)f_\mathrm{B}(E_\mathbf{q})/E_\mathbf{q}$ is the thermal one [37].

We note in passing that Eq. (26) is consistent with the so-called SF weight that is derived in Refs. [11,12] for a multiband Bloch Hamiltonian (see also [13]). Unlike our phase-twist method, they define the SF weight as the long-wavelength and zero-frequency limit of the current-current linear response. In particular our expression for a continuum model is formally equivalent to their $D_{1,\mu\nu}^s+D_{2,\mu\nu}^s+D_{3,\mu\nu}^s$ with the caveat that $D_{2,\mu\nu}^s$ is canceled by the interband contribution of $D_{1,\mu\nu}^s$. This is similar to the cancellation that they observed for the kagome lattice. Furthermore, Eq. (26) can also be split into two parts, $\rho_{ij}=\rho_{ij}^\mathrm{intra}+\rho_{ij}^\mathrm{inter}$, depending

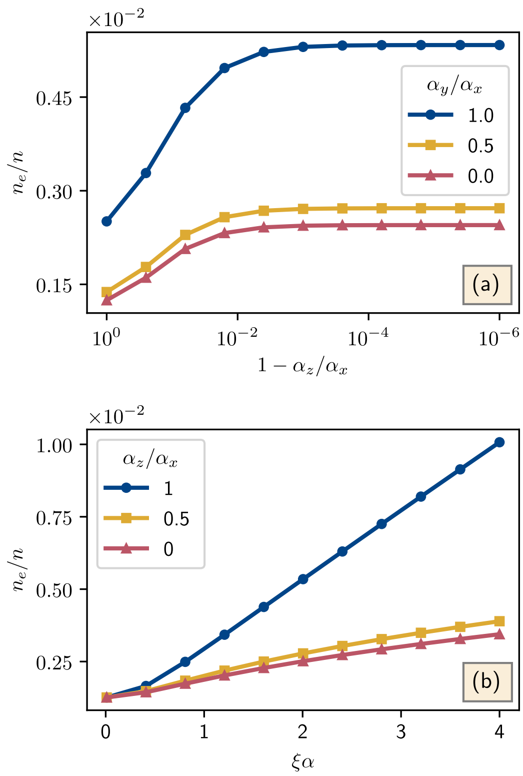

FIG. 4. Quantum depletion of the condensate density is shown as a function of SOC parameters when $T = 0$ and $U = U_{\uparrow\uparrow} = U_{\downarrow\downarrow} = 10U_{\uparrow\downarrow}/9$. The fraction of the depletion is plotted (a) as a function of α_z for three values of α_y when $\alpha_x = 2/\xi$ is fixed and (b) as a function of the SOC strength $\alpha = \alpha_x = \alpha_y$ for three values of the α_z/α ratio.

on the physical origin of the terms [11,12]: the intraband (interband) processes give rise to the conventional (geometric) contribution. This division is motivated by the success of a similar description with Fermi SFs [3,7].

In order to provide further evidence for its geometric origin, in Fig. 3 we compare the interband contribution with that of the intraband one coming from the summation term in Eq. (26). Here we set $T \to 0$. First of all, Fig. 3 shows that the total contribution from the summation term decreases with the increased strength and isotropy of the SOC fields, i.e., when $\alpha_y \to \alpha_x$ in Figs. 3(a)–3(c) and when $\alpha_z \to \alpha$ in Figs. 3(d)–3(f). Thus, ρ_{xx} always decreases from n_t with SOC. However, depending on the value of α_y and α_z, the remaining contribution $n_e + n_0(\alpha_x^2 - \alpha_y^2\delta_{iy} - \alpha_z^2\delta_{iz})/\alpha_x^2$ to ρ_{yy} and ρ_{zz} in Eq. (26) may compete with or favor the contribution from the summation term. More importantly, Fig. 3 shows that not only does ρ_{zz} have the largest interband contribution but also its relative weight is predominantly controlled by $\alpha_z \neq 0$. These findings support our Bogoliubov dispersion given in Eq. (20), whose quantum-geometric contributions are fully controlled by $\alpha_z \neq 0$. For completeness, in Fig. 4 we present the quantum depletion n_e^0 as a function of SOC parameters when $U = U_{\uparrow\uparrow} = U_{\downarrow\downarrow} = 10U_{\uparrow\downarrow}/9$. Figure 4 shows that n_e^0 increases with the increased strength and isotropy of the SOC fields [18], i.e., when $\alpha_y \to \alpha_x$ in Fig. 4(a) and when $\alpha_z \to \alpha$ in Fig. 4(b). This is clearly a direct consequence of the increased degeneracy of the single-particle spectrum. However, since $n_e^0 \ll n$ even for moderately strong SOC fields, the Bogoliubov approximation is expected to work well in general.

V. CONCLUSION

To summarize here we considered the plane-wave BEC phase of a spin-orbit-coupled Bose gas and reexamined its SF properties from a quantum-geometric perspective. In order to achieve this task analytically, we first reduced the 4×4 Bogoliubov Hamiltonian (which involves both lower and upper helicity bands) down to 2×2 by projecting the system onto the lower helicity band. This was motivated by the assumption that the energy gap between the lower and upper helicity bands near the single-particle ground state is much larger than the interaction energy. Then, given our numerical verification that the projected Hamiltonian provides an almost perfect description of the lower (higher) quasiparticle (quasihole) branch in the Bogoliubov spectrum, we exploited the low-momentum Bogoliubov spectrum analytically and identified the geometric contributions to the sound velocity. In contrast to the conventional contribution that has square-root dependence on the interaction strength, we found that the geometric ones are distinguished by linear dependence. It may be important to emphasize that these geometric effects are not caused by the negligence of the upper helicity band. Similar to the fermion problem where the geometric effects dress the effective mass of the Goldstone modes [5,6], here one can also interpret the geometric terms in terms of a dressed effective mass for the Bogoliubov modes. We also discussed the roton instability of the plane-wave ground state against the stripe phase and determined the phase-transition boundary. In addition we derived the SF density tensor by imposing a phase twist on the condensate order parameter and analyzed the relative importance of its contribution from the interband processes that is related to the quantum geometry. Looking forward, we believe it will be worthwhile to do a similar analysis for the stripe phase.

ACKNOWLEDGMENTS

We thank A. Julku for email correspondence, and M.I. acknowledges funding from TÜBİTAK Grant No. 1001-118F359.

[1] S. Peotta and P. Törmä, Superfluidity in topologically nontrivial flat bands, Nat. Commun. **6**, 8944 (2015).

[2] L. Liang, T. I. Vanhala, S. Peotta, T. Siro, A. Harju, and P. Törmä, Band geometry, Berry curvature, and superfluid weight, Phys. Rev. B **95**, 024515 (2017).

[3] M. Iskin, Exposing the quantum geometry of spin-orbit-coupled Fermi superfluids, Phys. Rev. A **97**, 063625 (2018).

[4] M. Iskin, Quantum metric contribution to the pair mass in spin-orbit-coupled Fermi superfluids, Phys. Rev. A **97**, 033625 (2018).

[5] M. Iskin, Geometric contribution to the Goldstone mode in spin-orbit-coupled Fermi superfluids, Phys. B (Amsterdam, Neth.) **592**, 412260 (2020).

[6] M. Iskin, Collective excitations of a BCS superfluid in the presence of two sublattices, Phys. Rev. A **101**, 053631 (2020).

[7] A. Julku, L. Liang, and P. Törmä, Superfluid weight and Berezinskii-Kosterlitz-Thouless temperature of spin-imbalanced and spin-orbit-coupled Fulde-Ferrell phases in lattice systems, New J. Phys. **20**, 085004 (2018).

[8] Z. Wang, G. Chaudhary, Q. Chen, and K. Levin, Quantum geometric contributions to the BKT transition: Beyond mean field theory, Phys. Rev. B **102**, 184504 (2020).

[9] P. Törmä, L. Liang, and S. Peotta, Quantum metric and effective mass of a two-body bound state in a flat band, Phys. Rev. B **98**, 220511(R) (2018).

[10] M. Iskin, Two-body problem in a multiband lattice and the role of quantum geometry, Phys. Rev. A **103**, 053311 (2021). See also Effective-mass tensor of the two-body bound states and the quantum-metric tensor of the underlying Bloch states, arXiv:2109.06000 [Phys. Rev. A (to be published)].

[11] A. Julku, G. M. Bruun, and P. Törmä, Quantum Geometry and Flat Band Bose-Einstein Condensation, Phys. Rev. Lett. **127**, 170404 (2021).

[12] A. Julku, G. M. Bruun, and P. Törmä, Excitations of a Bose-Einstein condensate and the quantum geometry of a flat band, Phys. Rev. B **104**, 144507 (2021).

[13] Recently, we became aware of an independent study [14] in which the SF density tensor is derived for a two-dimensional system using the linear-response theory. The results seem to agree with ours when there is an overlap.

[14] L. Yang, Quantum-fluctuation-induced superfluid density in two-dimensional spin-orbit-coupled Bose-Einstein condensates, Phys. Rev. A **104**, 023320 (2021).

[15] Y. Li, G. I. Martone, and S. Stringari, Bose-Einstein condensation with spin-orbit coupling, *Annual Review of Cold Atoms and Molecules*, Vol. 3 (World Scientific, 2015), Chap. 5, pp. 201–250.

[16] H. Zhai, Degenerate quantum gases with spin-orbit coupling: A review, Rep. Prog. Phys. **78**, 026001 (2015).

[17] Y. Zhang, M. E. Mossman, T. Busch, P. Engels, and C. Zhang, Properties of spin-orbit-coupled Bose-Einstein condensates, Front. Phys. **11**, 118103 (2016).

[18] X. Cui and Q. Zhou, Enhancement of condensate depletion due to spin-orbit coupling, Phys. Rev. A **87**, 031604(R) (2013).

[19] T. Ozawa and G. Baym, Stability of Ultracold Atomic Bose Condensates with Rashba Spin-Orbit Coupling against Quantum and Thermal Fluctuations, Phys. Rev. Lett. **109**, 025301 (2012).

[20] G. Baym and T. Ozawa, Condensation of bosons with Rashba-Dresselhaus spin-orbit coupling, J. Phys.: Conf. Ser. **529**, 012006 (2014).

[21] C. Wang, C. Gao, C.-M. Jian, and H. Zhai, Spin-Orbit Coupled Spinor Bose-Einstein Condensates, Phys. Rev. Lett. **105**, 160403 (2010).

[22] R. Barnett, S. Powell, T. Graß, M. Lewenstein, and S. Das Sarma, Order by disorder in spin-orbit-coupled Bose-Einstein condensates, Phys. Rev. A **85**, 023615 (2012).

[23] L. Santos, G. V. Shlyapnikov, and M. Lewenstein, Roton-Maxon Spectrum and Stability of Trapped Dipolar Bose-Einstein Condensates, Phys. Rev. Lett. **90**, 250403 (2003).

[24] S. Saccani, S. Moroni, and M. Boninsegni, Excitation Spectrum of a Supersolid, Phys. Rev. Lett. **108**, 175301 (2012).

[25] T. Macrì, F. Maucher, F. Cinti, and T. Pohl, Elementary excitations of ultracold soft-core bosons across the superfluid-supersolid phase transition, Phys. Rev. A **87**, 061602(R) (2013).

[26] J.-N. Schmidt, J. Hertkorn, M. Guo, F. Böttcher, M. Schmidt, K. S. H. Ng, S. D. Graham, T. Langen, M. Zwierlein, and T. Pfau, Roton Excitations in an Oblate Dipolar Quantum Gas, Phys. Rev. Lett. **126**, 193002 (2021).

[27] F. Böttcher, J.-N. Schmidt, J. Hertkorn, K. S. H. Ng, S. D. Graham, M. Guo, T. Langen, and T. Pfau, New states of matter with fine-tuned interactions: Quantum droplets and dipolar supersolids, Rep. Prog. Phys. **84**, 012403 (2021).

[28] M. A. Khamehchi, Y. Zhang, C. Hamner, T. Busch, and P. Engels, Measurement of collective excitations in a spin-orbit-coupled Bose-Einstein condensate, Phys. Rev. A **90**, 063624 (2014).

[29] S.-C. Ji, L. Zhang, X.-T. Xu, Z. Wu, Y. Deng, S. Chen, and J.-W. Pan, Softening of Roton and Phonon Modes in a Bose-Einstein Condensate with Spin-Orbit Coupling, Phys. Rev. Lett. **114**, 105301 (2015).

[30] J.-R. Li, J. Lee, W. Huang, S. Burchesky, B. Shteynas, F. C. Top, A. O. Jamison, and W. Ketterle, A stripe phase with supersolid properties in spin-orbit-coupled Bose-Einstein condensates, Nature (London) **543**, 91 (2017).

[31] A. Putra, F. S.- Cárcoba, Y. Yue, S. Sugawa, and I. B. Spielman, Spatial Coherence of Spin-Orbit-Coupled Bose Gases, Phys. Rev. Lett. **124**, 053605 (2020).

[32] Y. Li, G. I. Martone, L. P. Pitaevskii, and S. Stringari, Superstripes and the Excitation Spectrum of a Spin-Orbit-Coupled Bose-Einstein Condensate, Phys. Rev. Lett. **110**, 235302 (2013). See also the more recent analysis by G. I. Martone and S. Stringari, Supersolid phase of a spin-orbit-coupled Bose-Einstein condensate: A perturbation approach, SciPost Phys. **11**, 092 (2021).

[33] Y.-C. Zhang, Z.-Q. Yu, T. K. Ng, S. Zhang, L. Pitaevskii, and S. Stringari, Superfluid density of a spin-orbit-coupled Bose gas, Phys. Rev. A **94**, 033635 (2016)

[34] X.-L. Chen, J. Wang, Y. Li, X.-J. Liu, and H. Hu, Quantum depletion and superfluid density of a supersolid in Raman spin-orbit-coupled Bose gases, Phys. Rev. A **98**, 013614 (2018).

[35] E. Taylor, A. Griffin, N. Fukushima, and Y. Ohashi, Pairing fluctuations and the superfluid density through the BCS-BEC crossover, Phys. Rev. A **74**, 063626 (2006).

[36] L. He and X.-G. Huang, BCS-BEC crossover in three-dimensional Fermi gases with spherical spin-orbit coupling, Phys. Rev. B **86**, 014511 (2012).

[37] A. L. Fetter and J. D. Walecka, *Quantum Theory of Many-Particle Systems* (McGraw-Hill, New York, 1971).